

A Comparative Study of Fracture Toughness at Cryogenic Temperature of Austenitic Stainless Steel Welds

I. Aviles Santillana, C. Boyer, P. Fernandez Pison, A. Foussat, S.A.E. Langeslag, A.T. Perez Fontenla, E.M. Ruiz Navas, and S. Sgobba

(Submitted May 25, 2017; in revised form February 1, 2018; published online March 6, 2018)

The ITER magnet system is based on the “cable-in-conduit” conductor (CICC) concept, which consists of stainless steel jackets filled with superconducting strands. The jackets provide high strength, limited fatigue crack growth rate and fracture toughness properties to counteract the high stress imposed by, among others, electromagnetic loads at cryogenic temperature. Austenitic nitrogen-strengthened stainless steels have been chosen as base material for the jackets of the central solenoid and the toroidal field system, for which an extensive set of cryogenic mechanical property data are readily available. However, little is published for their welded joints, and their specific performance when considering different combinations of parent and filler metals. Moreover, the impact of post-weld heat treatments that are required for Nb₃Sn formation is not extensively treated. Welds are frequently responsible for cracks initiated and propagated by fatigue during service, causing structural failure. It becomes thus essential to select the most suitable combination of parent and filler material and to assess their performance in terms of strength and crack propagation at operation conditions. An extensive test campaign has been conducted at 7 K comparing tungsten inert gas (TIG) welds using two fillers adapted to cryogenic service, EN 1.4453 and JK2LB, applied to two different base metals, AISI 316L and 316LN. A large set of fracture toughness data are presented, and the detrimental effect on fracture toughness of post-weld heat treatments (unavoidable for some of the components) is demonstrated. In this study, austenitic stainless steel TIG welds with various filler metals have undergone a comprehensive fracture mechanics characterization at 7 K. These results are directly exploitable and contribute to the cryogenic fracture mechanics properties database of the ITER magnet system. Additionally, a correlation between the impact in fracture toughness and microstructure resulting from the above treatment is provided.

Keywords austenitic stainless steel, cryogenic, fracture toughness, secondary phases, welding

1. Introduction

The ITER project aims to build a fusion reactor, with the goal of demonstrating the scientific and technical feasibility of fusion power (Ref 1). It is a joint project between the European Union, China, India, Japan, South Korea, the Russian Federation and the USA. It will allow the study of plasmas in conditions similar to those expected in an electricity-generating fusion power plant. It is designed to generate 500 MW of fusion power for extended periods of time, ten times more than the energy input needed to keep the plasma at the right temperature. It will therefore be the first fusion experiment to produce net power (Ref 1).

ITER is based on the “tokamak” concept—a donut-shaped vessel surrounded by coils that produce an intense magnetic field—in which the conditions needed for nuclear fusion are created and maintained (Ref 1). The ITER tokamak requires a

superconducting magnet system in order to form, control and drive the plasma. It is divided into four main sub-systems: 18 toroidal field (TF) coils; the central solenoid (CS); 6 poloidal field (PF) coils; and 9 pairs of correction coils (CCs) (Ref 2). These superconducting magnets are cooled with supercritical helium at 4.2 K (Ref 2). The high thermal contractions during cool down from 300 K to operation temperature together with large Lorentz forces will result in highly stressed components (Ref 3). It turns out essential a comprehensive assessment of the mechanical properties of its components under conditions approaching those when operating, in particular those of the welds for which much less has been published. This work is devoted to the study of the fracture toughness as it has been identified as a paramount mechanical property in order to implement a fracture mechanics approach to design (Ref 4-6).

Measurements of fracture toughness K_{IC} are based on linear-elastic fracture mechanics (LEFM) (Ref 6). Nevertheless, austenitic stainless steel used for cryogenic applications is in the range of intermediate-strength high toughness engineering materials. Considering the size of the plastic region at the end of the crack tip with respect to the size of our sample, LEFM is no longer applicable. An alternative test method based on elastic-plastic fracture mechanics (EPFM) and the Rice’s J -integral concept (Ref 7) is more suitable and therefore applied here.

2. Materials

Austenitic stainless steels have been chosen as the baseline for the jackets of the “cable-in-conduit” conductors (CICC) mainly due to their high strength and low magnetic permeabil-

I. Aviles Santillana, CERN, 1211 Geneva, Switzerland; and University Carlos III of Madrid, Campus de Leganes, Av. Universidad 30, 28911 Madrid, Spain; C. Boyer and A. Foussat, ITER Organization, Route de Vinon sur Verdon, CS 90 046, 13067 St. Paul lez Durance Cedex, France; P. Fernandez Pison, S.A.E. Langeslag, A.T. Perez Fontenla, and S. Sgobba, CERN, 1211 Geneva, Switzerland; and E.M. Ruiz Navas, University Carlos III of Madrid, Campus de Leganes, Av. Universidad 30, 28911 Madrid, Spain. Contact e-mail: Ignacio.Aviles.Santillana@cern.ch.

ity at operating temperature. The varying jackets for the different magnet components are manufactured from advanced austenitic stainless steel grades such as AISI 316L and AISI 316LN. For the transitions between them and to feeder connections, tungsten inert gas (TIG) welds are carried out, for which the filler metals are currently under study.

Due to the extremely high currents the cables need to transport [nominally up to 68 kA (Ref 3)], some of the sub-systems (TF coils and the CS) are fabricated with Nb₃Sn strands, which need to undergo a reaction heat treatment (650 °C, 200 h) after their insertion in the circular jacket (Fig. 1) and successive coiling operation. This heat treatment could have a strong impact in the mechanical behavior of the jackets and its welded joints and justifies the goal of the added study in heat treatment effects.

The materials which were used for the study consist of different grades of austenitic stainless steel. For the base material, AISI 316L and AISI 316LN were employed. Premium grades of these austenitic types are used, with a mandatory electroslag remelting (ESR) step to reduce impurity contents (P and S) to the minimum in order to avoid hot cracking susceptibility (Ref 8, 9). Additionally, very stringent requirements in terms of inclusions [macroinclusions are strictly forbidden and for microinclusions severity level shall be at most 2 as for method D described in ASTM E45 (Ref 10)] and magnetic permeability ($\mu_r < 1.005$ for fields over 80,000 A/m) have to be respected. For the filler metals, a commercial alloy was used (EN 1.4453, AWS ER317LN) together with a high manganese alloy (JK2LB), specially conceived to withstand the reaction heat treatment to which the jackets are submitted (Ref 11-13).

3. Experimental

3.1 Welding

The weld plates were all prepared at CERN based on an existing welding procedure specification. The dimensions of the plates to be used as base material were chosen to fulfill standard ISO 15614 (Ref 14), which defines the conditions for the execution of welding procedure tests and the range of qualification for arc and gas welding operations of steels. Six-mm-thick plates were welded and afterward machined down to 4 mm by removing 1 mm from each side.

The joint is a full penetration butt weld (BW) with a flat position [flat-PA according to ISO 6947 (Ref 15)] in a “V”

configuration of 90°, performed from one side without backing as depicted in Fig. 2(a). The process utilized is tungsten inert gas (TIG) with filler metal [142 according to ISO 4063 (Ref 16)]. The gas used for the shielding was argon. Every weld was done in three passes (Fig. 2b), with the gas flow always kept at 10 L/min. A negative polarity on the cathode and direct current was used in order to produce a narrow arc and thus a narrow weld bead.

The compact tension (CT) specimens of 4 mm thickness are machined from the mid-part of the welded plates according to standard ASTM E1820-01 (Ref 17). The notch tip of all specimens was in the middle of the weld zone. Crack propagation and extension are prepared to coincide with the weld axis, in longitudinal orientation [T–L orientation according to ASTM 1823 (Ref 18)].

3.2 Heat Treatment

In order to assess the impact of the reaction heat treatment on the weld properties, part of the weld plates were submitted to a heat cycle which was adapted to CERN’s vacuum furnace to fulfill ITER’s requirements. The cycle conditions consisted on a heating rate of 5 °C/h followed by a plateau of 200 h at 650 °C. They are cooled via natural convection at a speed of approximately 30 °C/h. This heat treatment is done under vacuum (10⁻⁶ mbar) to mimic the conditions of the reaction of the Nb₃Sn superconducting strands.

3.3 Fracture Toughness

A total of 12 CT specimens (two specimens per group sample) without side grooves have been tested with different combinations of base material, filler and heat treatment. It was confirmed after failure that the crack was kept confined inside the weld bead at every moment, and thus, the properties which are measured correspond to the ones of the weld bead. Table 1 shows a summary of all the specimens which were tested. For the sample designation, the first letter corresponds to the base material (L or LN); next to it, there is a reference to the filler material (4453 or JK2LB). The last part refers to the fact that the samples have been heat-treated (HTR) or not (NHT).

All the measurements were taken at 7 K, slightly above the foreseen operating temperature, however, which allows for the measurement in a dry environment. The impact of this 3 K difference in mechanical properties is considered to be negligible. In order to reach such a low temperature, samples are tested in a temperature-controlled cryostat, equipped with resistors and temperature sensors. A controlled flow of helium gas and several sets of resistors connected with a feedback loop

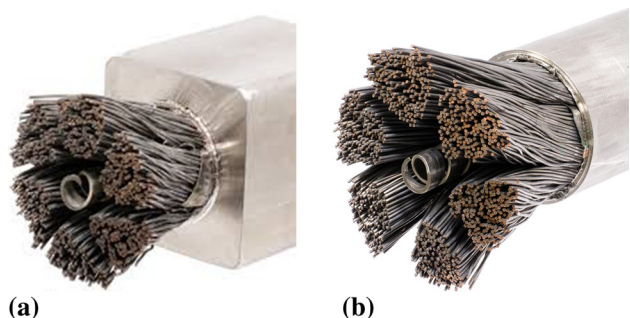


Fig. 1 Typical ITER cable-in-conduit conductors. (a) Central Solenoid (CS); (b) toroidal field (TF)

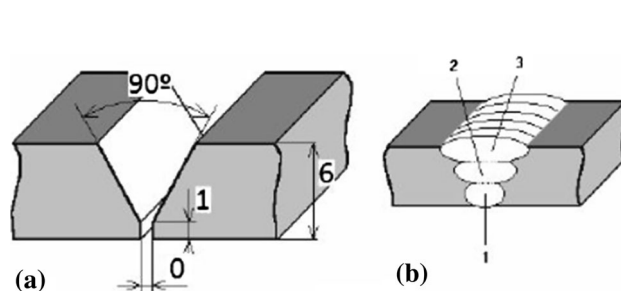


Fig. 2 (a) Sketch of the weld joint before welding procedure. Units in mm; (b) sketch of the weld joint after the welding procedure showing the three passes

Table 1 Summary table of the sample designation

Group sample designation	Base material	Filler metal	Heat treatment
L-4453-NHT	316L	EN 1.4453	No
L-4453-HTR	316L	EN 1.4453	650 °C/200 h
LN-4453-NHT	316LN	EN 1.4453	No
LN-4453-HTR	316LN	EN 1.4453	650 °C/200 h
LN-JK2LB-NHT	316LN	JK2LB	No
LN-JK2LB-HTR	316LN	JK2LB	650 °C/200 h

to the temperature sensors guarantee a constant temperature of 7 K along the duration of the tests.

Precracking was performed according to ASTM E1820 at 7 K. A frequency of 15 Hz was used to avoid heating of the specimen. To follow crack-tip position, an extensometer was fixed at the load line of the compact tension specimen both during precracking and during fracture testing. A load control was put in place for the precracking. After precracking, the load ratio is adjusted to reach around $\Delta K = 20 \text{ MPa}\sqrt{\text{m}}$ until a crack size of around 2 mm was reached. The unloading compliance method was used in order to obtain a load–load line displacement (LLD) curve which was plotted for each one of the samples (Fig. 3a). It is used to build the J – Δa curve (Fig. 3b) from which the toughness parameters are obtained. The blunting line (straight line on the left of Fig. 3b) is calculated from the material's tensile properties as:

$$J = 2\sigma_y\Delta a \quad (\text{Eq 1})$$

The data points obtained from the load–LLD curve are fitted to a power-law regression as observed in Fig. 3(b). The intersection between the regression line and the blunting line gives a candidate J_Q , which becomes J_{IC} if the validity requirements described in ASTM 1820:01 (Ref 17) are fulfilled. The results of the assessment of the J – Δa curves are given in Table 2, where the values for J_Q are gathered. Additionally, it contains the K_{JIC} values for information as not all specimens fulfill the size requirements imposed in ASTM E1820. The material properties used to assess the validity requirements and to draw the blunting line were obtained from (Ref 11) for samples using JK2LB as filler material and from (Ref 19) for the samples using EN 1.4453. However, the validity criterion according to crack front is always fulfilled as it can be observed in the macrofractograph after testing sample L-4453-HTR shown in Fig. 4.

The requirements for fracture toughness on the welds found in the ITER procurement arrangement for the toroidal magnets are determined in terms of K_{JIC} . Thus, taking this into account, equivalence between J_Q and K_{JIC} is found in (Ref 20) through Eq 2.

$$K_{JIC} = \sqrt{\frac{E \cdot J_Q}{(1 - \nu^2)}} \quad (\text{Eq 2})$$

where E is the Young's modulus of the stainless steel and ν its Poisson's ratio at the testing temperature.

3.4 Microstructural and Fractographic Study: Secondary Phases Quantification

The presence of phases other than austenite in the welded components is of great concern due to its brittleness at 7 K. Metallographic examinations of the different combinations of

base and filler material were carried out both before and after heat treatment with a Carl–Zeiss SIGMA SEM and a backscattered electron detector in order to identify and quantify them. This work is focused on the quantification of δ -ferrite and σ -phase. The technique that has been considered to be the most suitable for their quantification is scanning electron microscope (SEM) analysis via backscattered electron (BSE) detector as it displays an excellent lateral resolution ($< 1 \mu\text{m}$) and sufficient contrast between the phases to perform a subsequent image analysis (Ref 21). Ten images were obtained in the weld bead for every combination of base and filler material before and after heat treatment, more accurately, in the region depicted in Fig. 5. BSE images were subsequently analyzed with a professional image analysis software (AxioVision[®]), which is able to discriminate the different levels of gray that can be attributed to austenite, δ -ferrite and σ -phase (Ref 21).

SEM fractographies on failed specimens to delineate the differences in the fracture behaviors have been performed with the same microscope, using, however, a secondary electron detector. The fracture modes as well as other relevant characteristics have been identified.

Bearing in mind that during the fracture mechanics tests, the crack initiation, propagation and opening happens inside the weld bead, phase quantification was performed exclusively there in order to be able to find a correlation between fracture toughness at cryogenic temperature and the occurrence of brittle secondary phases.

4. Results

4.1 Fracture Toughness

An assessment of the resistance curves that were plotted for every specimen yields the results of J_Q together with the K_{JIC} values (calculated through Eq 2), which are gathered in Table 2. It is already quite evident that the samples before heat treatment (NHT) exhibit higher values than after it (HTR). A better performance of the filler JK2LB with respect to EN 1.4453 is also observed. In Table 2, it can also be seen a better mechanical behavior of equivalent group of samples when 316LN is used as base material.

4.2 Secondary Phases Quantification

δ -Ferrite and σ -phase were successfully identified as shown in Fig. 4. The differences in composition of the secondary phases with respect to the austenitic matrix make it possible to differentiate them. Figure 6 shows white regions embedded in the austenitic matrix correspond to Mo-rich σ -phase and darker regions correspond to δ -ferrite (enriched in Cr and containing

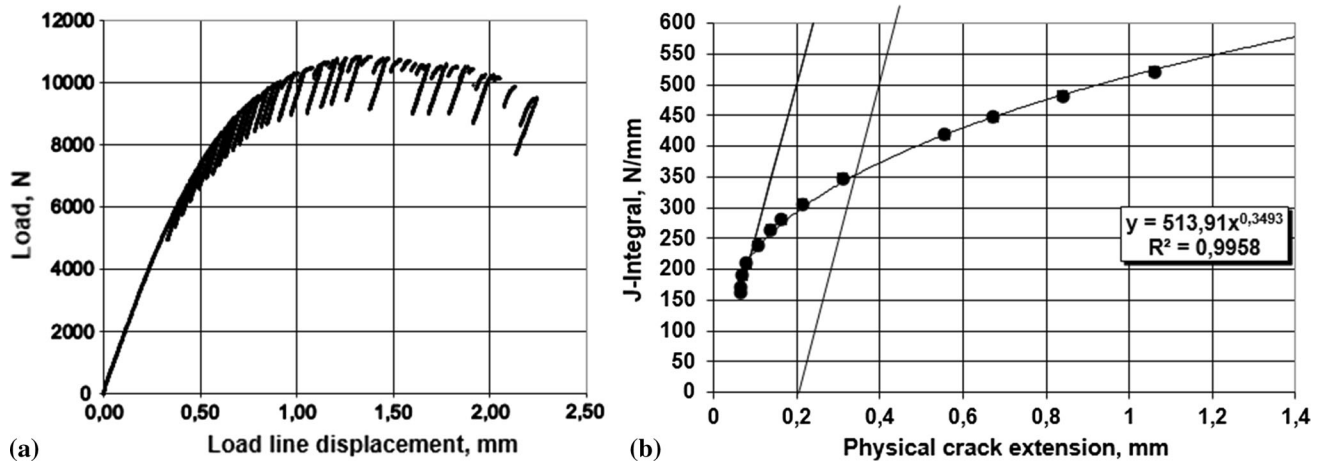


Fig. 3 (a) Load-LLD curve (10% unloading) for sample LN-JK2LB-NHT; (b) $J-\Delta a$ curve for sample LN-JK2LB-NHT

Table 2 Testing results of fracture toughness for the different combinations of base material, filler metal and heat treatment

Sample designation	J_Q , kJ/m ²	K_{JIC} , MPa√m
L-4453-NHT	252 ± 14	238 ± 6
L-4453-HTR	78 ± 8	132 ± 7
LN-4453-NHT	345 ± 0	262 ± 0
LN-4453-HTR	107 ± 17	151 ± 17
LN-JK2LB-NHT	355 ± 5	266 ± 1
LN-JK2LB-HTR	269 ± 9	232 ± 4

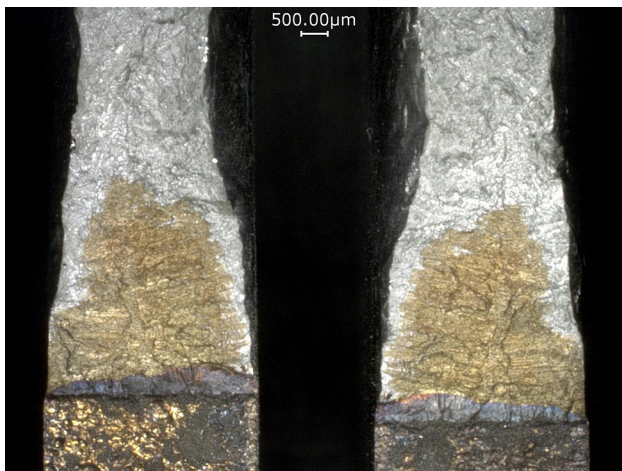


Fig. 4 Macrofractograph of broken sample L-4453-HTR

less Ni with respect to the austenitic matrix) and an austenitic matrix in gray.

With the subsequent image analysis, a quantification of δ -ferrite and σ -phase was performed for each combination of base material, filler metal and heat treatment, in 10 random locations inside the weld bead. The results are shown in Table 3 in area %, representing the ratio between the total surface covered by each phase in the 10 fields which were analyzed and the total surface. It is already evident that the amount of secondary phases when using 316L as base material is higher than when using 316LN. Samples where JK2LB was used as

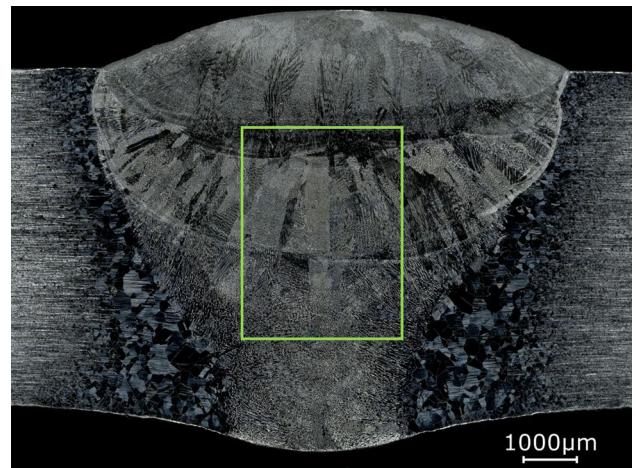


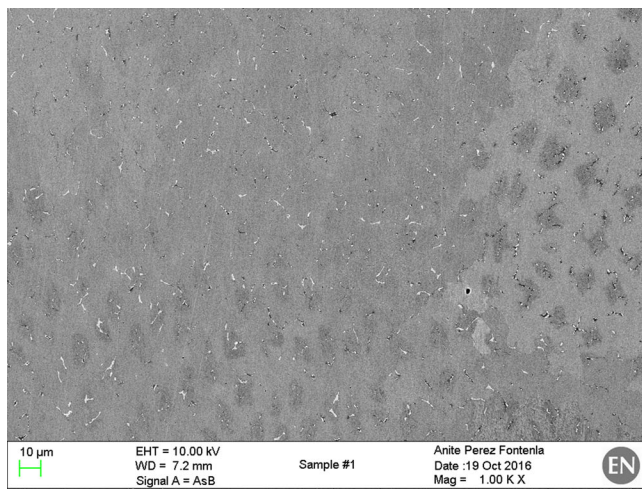
Fig. 5 Macrograph of sample L-4453-NHT after oxalic acid etching. The green rectangle (3 mm × 4 mm) shows the region where the 10 fields for the phase analysis were taken, corresponding to the region where the crack was propagating

filler material show an extremely low quantity of secondary phases.

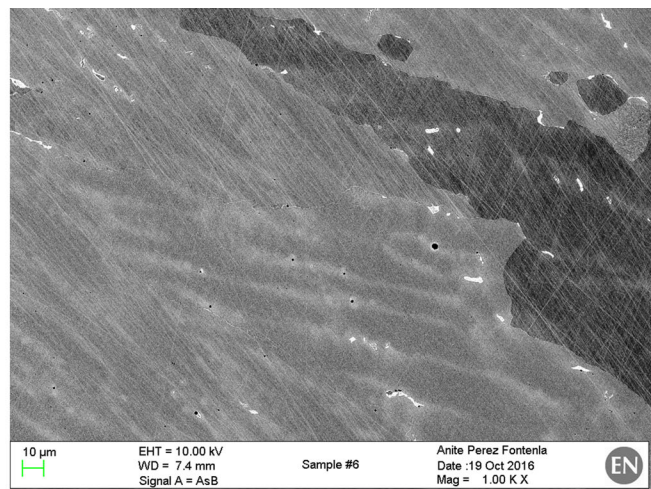
The fractographic studies carried out at the broken surfaces of the CT specimens show that, for the samples which were not subject to the reaction heat treatment, a ductile failure mode is generally observed (Fig. 7). The rupture facies is populated by equiaxial dimples, as a consequence of microvoid coalescence. On the other hand, observation of the broken CT samples after reaction heat treatment shows, apart from local ductility (dimples), a more faceted surface (Fig. 8). In addition, what is of most interest is the fractured brittle phases embedded in the matrix (Fig. 8).

5. Discussion of the Results

As it has already been stated, even if the validity according to crack front is successfully achieved, the size of our specimens does not fulfill size criterion required in ASTM 1820. The toughness values herein studied are for a three-pass TIG manual weld of 4 mm thickness. Their equiv-



(a)



(b)

Fig. 6 Backscattered electron images of the weld bead of sample L-4453-NHT (a) and sample L-4453-HTR (b). White regions embedded in the austenitic matrix correspond to Mo-rich σ -phase, whereas darker regions correspond to δ -ferrite (enriched in Cr and containing less Ni with respect to the austenitic matrix in gray)

Table 3 Secondary phase quantification via SEM and image analysis

Sample designation	δ -Ferrite (area %)	σ -Phase (area %)
L-4453-NHT	0.31	0.84
L-4453-HTR	0.24	1.00
LN-4453-NHT	0.01	0.05
LN-4453-HTR	0.00	0.11
LN-JK2LB-NHT	0.00	0.00
LN-JK2LB-HTR	0.00	0.01

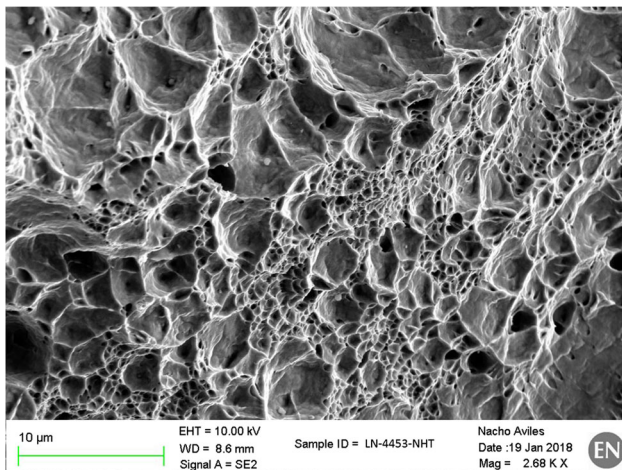


Fig. 7 Secondary electron image of broken CT specimen (LN-4453-NHT). Equiaxial dimples denoting ductility. Original magnification: $\times 2000$

alent K_{JIC} values are shown for information and comparison. Toughness data obtained using such specimens may not satisfy the validity criteria of tests standards and might be size dependent. However, the results are directly relevant for specific designs assuming that the specimen is identical in thickness to the intended service component. Additionally,

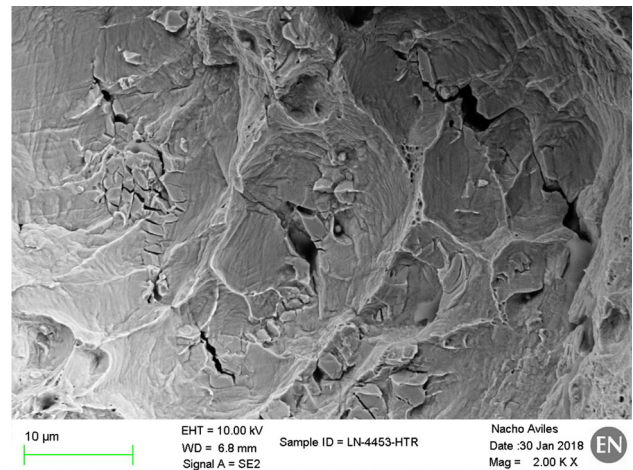


Fig. 8 Secondary electron image of broken CT specimen (LN-4453-HTR). Fractured brittle secondary phases embedded in the matrix are observed. Original magnification: $\times 2000$

ASTM intentionally chooses specimen configurations that maximize crack-tip constraint by using deeply cracked, relatively thick specimens to obtain conservative measurements of fracture toughness properties. In structural applications, the cracks are often small relative to other dimensions and often three-dimensional in shape and the loading can be predominantly tensile. These differences, alone or in combination, result in effectively tougher behavior, causing the direct application of ASTM fracture toughness measurements to structures to be conservative (Ref 20).

Based on the obtained results regarding the fracture toughness, it is noticeable that the reaction heat treatment has an important impact on the fracture toughness of the welds. There is always a clear reduction in this parameter following heat treatment independently of the combination of base material and filler metal used. Considering that the sensitization temperature for austenitic stainless steels is between 425 and

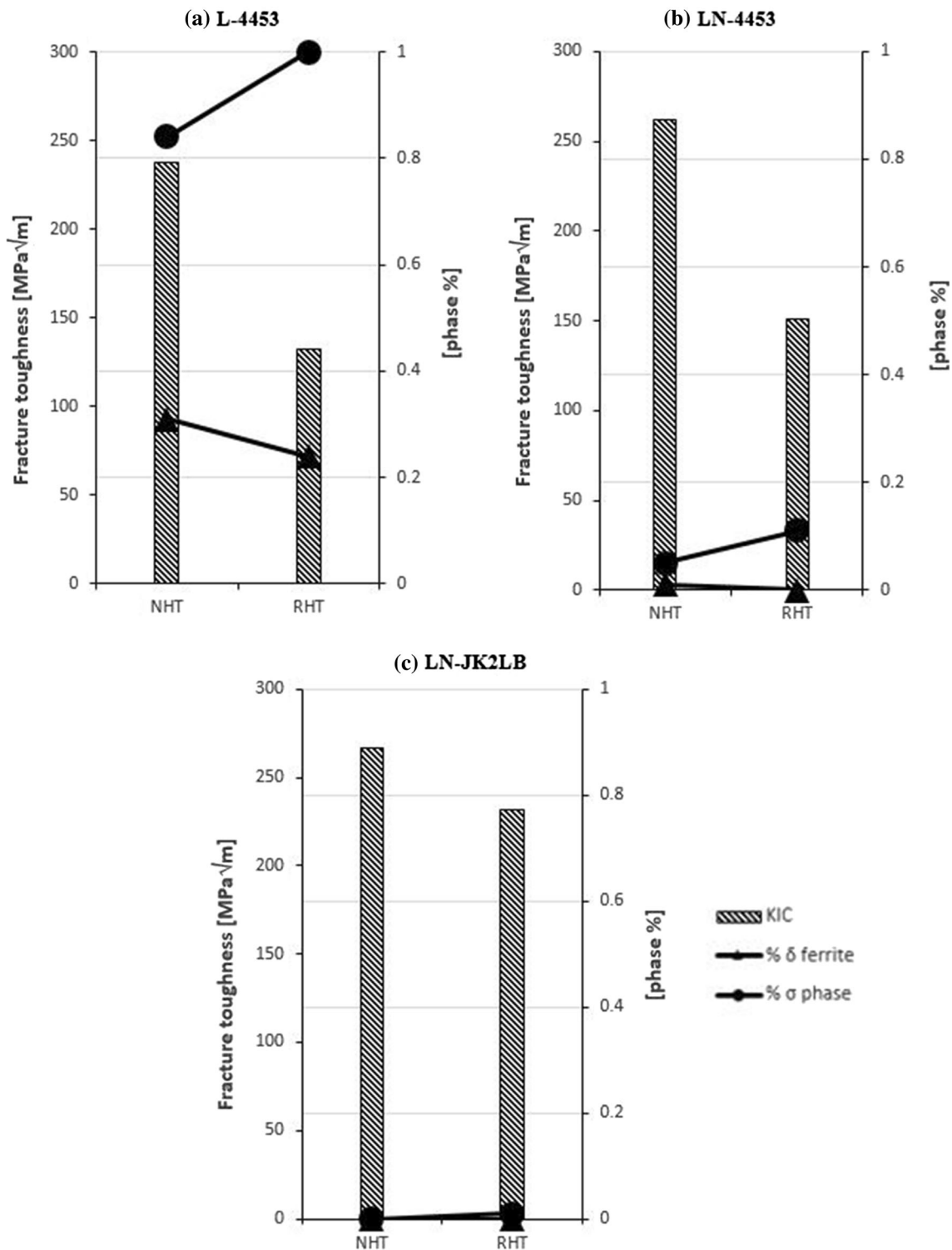


Fig. 9 Fracture toughness and phase % of the different combinations of base material and filler material both before (NHT) and after (RHT) heat treatment. (a) 316L + 1.4453; (b) 316LN + 1.4453; (c) 316LN + JK2LB

815 °C (Ref 22, 23), precipitation of carbides in grain boundaries after 200 h at 650 °C is to be expected and needs to be further studied. Moreover, the two filler metals studied possess non-negligible quantities of nitrogen, which makes the precipitation of chromium nitrides in grain boundaries also likely to happen (Ref 23). Both processes significantly lower the fracture toughness as it is observed.

To the extent of the performed analyses, better results are achieved when using AISI 316LN as base material with respect to AISI 316L. Fracture toughness of the untreated samples is higher, and the reduction in this value after heat treatment is lower. The more favorable behavior of AISI 316LN can be partly explained by dilution of base material and filler metal and a more favorable composition. The lower quantity of δ-

ferrite and σ -phase observed when 316LN is the base material (Table 3) backs up this thesis.

Based on the obtained results, using JK2LB as filler metal yields a higher fracture toughness after heat treatment than using EN 1.4453. This result is consistent with the fact that the alloy has been specifically tailored to withstand the reaction cycle, and with the minor quantity of δ -ferrite and σ -phase observed for JK2LB with respect to the higher quantities observed when using 1.4453 as a filler metal. However, considering that the specified value for fracture toughness is $130 \text{ MPa}\sqrt{\text{m}}$, EN 1.4453 provides generally satisfactory results and it has associated advantages with respect to JK2LB such as matching properties between filler and base material, ready and operational weldability, and a better matching thermal contraction down to 4 K.

SEM analysis combined with image analysis is considered to be a suitable technique to quantify the δ -ferrite and σ -phase of austenitic stainless steel welds, where the occurrence of these phases is very low ($< 2\%$). However, a fairly large scatter was observed after averaging the values of the 10 fields which were analyzed, which indicates that their distribution is highly heterogeneous as it has been already shown in (Ref 22). Hence, more fields should be studied and an assessment of the distribution of the phases in the weld bead is recommended.

A fairly good correlation between the fracture toughness at cryogenic temperature and the quantity of brittle secondary phases (δ -ferrite and σ -phase) is presented in Fig. 9, where it can be seen that the quantity of secondary phases is inversely proportional to the fracture toughness at cryogenic temperature. Additionally, an indication of the transformation of δ -ferrite to σ -phase is shown in Fig. 9, evidenced by the systematic increase in the latter in detriment of a decrease in the first after the heat treatment. This phase transformation driven by Cr diffusion during heat treatment has already been reported (Ref 24).

6. Conclusions

A comprehensive fracture mechanics characterization at 7 K of austenitic stainless steel TIG welds with various filler metals has been carried out, which brings about a contribution to the cryogenic mechanical properties knowledge and to the ITER magnet system material properties database.

The impact of unavoidable a post-weld heat treatment ($650 \text{ }^\circ\text{C}$, 200 h) has been addressed. A significant drop in fracture toughness after the heat treatment has been observed independently of the combination of base and filler material employed.

The study also shows a superior performance of AISI 316LN with respect to AISI 316L as base material in combination with the selected fillers. The fracture toughness of the first is superior to the latter before heat treatment, and the drop owed to the heat treatment is lower. The strengthening induced by the higher N content and the austenite stabilization (resulting in less occurrence of secondary phases) explain this behavior.

When comparing the two filler metals, JK2LB shows a higher fracture toughness after heat treatment than EN 1.4453, which is in good agreement with the fact that the composition of this material has been tailored to withstand the reaction heat treatment.

Secondary phases' (δ -ferrite and σ -phase) quantification shows a good correlation with the fracture toughness at cryogenic temperature, and an indication of the transformation of δ -ferrite to σ -phase is shown.

The fractographic analyses performed in the broken CT specimens show ductile characteristics (dimples) for the not heat-treated samples, which would imply a higher toughness of these specimens with respect to their heat-treated counterparts, showing not only a more faceted surface but also fractured brittle phases embedded in the austenitic matrix. This observations are thus in accordance with the secondary phase quantification and the mechanical testing results.

“The views and opinions expressed herein do not necessarily reflect those of the ITER Organization”.

Acknowledgments

The authors would like to express their thanks to Dr. Arman Nyilas (in memoriam) for the contributions made in this work.

References

1. *The ITER project*, European Fusion Development Agreement (EFDA) (2006)
2. Sborchia C. et al, *Overview of ITER Magnet System and European Contribution*, in 2011 IEEE/NPSS, 24th Symposium on Fusion Engineering
3. N. Mitchel et al., The ITER Magnets: Design and Construction Status, *IEEE Trans. Appl. Supercond.*, 2012, **22**(3), p 4200809
4. W.S. Pellini, *Guidelines for Fracture-Safe and Fatigue-Reliable Design of Steel Structures. Applications of Fracture Mechanics and Structural Integrity Technology*, Welding Institute, Cambridge, 1983
5. S.T. Rolfe and J.M. Barsom, *Fracture and Fatigue Control in Structures: Applications of Fracture Mechanics*, ASTM International, West Conshohocken, 1977
6. T.L. Anderson, *Fracture Mechanics: Fundamentals and Applications*, 3rd ed., CRC Press, Boston, 2005
7. J.R. Rice, A Path Independent Integral and the Approximate Analysis of Strain Concentration by Notched and Cracks, *Journal of Applied Mechanics*, 1968, **35**, p 379–386
8. V. Shankar, T.P.S. Gill, S.L. Mannan, and S. Sundaresan, Solidification Cracking in Austenitic Stainless Steel Welds, *Sadhana*, 2003, **28**(3–4), p 359–382
9. J.A. Brooks and A.W. Thompson, Microstructural Development and Solidification Cracking Susceptibility of Austenitic Stainless Steel Welds, *International Materials Reviews*, 1991, **36**(1), p 16–44
10. ASTM E45-13, Standard Test Methods for Determining the Inclusion Content of Steel
11. R.P. Walsh, V.J. Toplosky, K. Han, N.N. Martovetsky, T. Mann, and J.R. Miller, *Mechanical Properties of Modified JK2LB for Nb₃Sn CICC Applications*, CEC-ICMC, Tucson (Arizona), 2009
12. H. Nakajima et al., Development of Low Carbon and Boron Added 22Mn–13Cr–9Ni–1Mo–0.24N Steel (JK2LB) for Jacket which Undergoes Nb₃Sn Heat Treatment, *Trans. Appl. Superconduct.*, 2004, **14**(2), p 1145–1148
13. K. Hamada et al., Optimization of JK2LB Chemical Composition for ITER Central Solenoid Conduit Material, *Cryogenics*, 2007, **47**(3), p 174–182
14. ISO 15614-1:2004—Specification and qualification of welding procedures for metallic materials—Welding procedure test—Part 1: Arc and gas welding of steels and arc welding of nickel and nickel alloys
15. ISO 6947:2011—Welding and allied processes—Welding positions
16. ISO 4063:2009—Welding and allied processes—Nomenclature of processes and reference numbers
17. ASTM E1820:01—Standard Test Method for Measurement of Fracture Toughness
18. ASTM E1823—Standard Terminology Relating to Fatigue and Fracture Testing

19. K. Iida and A.J. McEvily, Ed., *Advanced Materials for Severe Service Applications*, Springer, Berlin, 2012
20. X.-K. Zhu and J.A. Joyce, Review of Fracture Toughness (G, K, J, CTOD, CTOA) Testing and Standardization, *Engineering Fracture Mechanics*, 2012, **85**, p 1–46
21. S. Kuimalee et al., Isothermal Phase Transformation Sequence in Fe–22wt%Cr–3.2wt%Mo–6.2wt%Ni–0.037%C Cast Duplex Stainless Steel, *Chiang Mai J. Sci.*, 2011, **38**(1), p 47–55
22. Y. Song, T.N. Baker, and N.A. McPherson, A Study of Precipitation 316LN Precipitation in As-Welded 316LN Plate Using 316L/317L Weld Metal, *Materials Science and Engineering: A*, 1996, **212**(2), p 228–234
23. Y. Zhou, Y. Liu, X. Zhou, C. Liu, J. Yu, Y. Huang et al., Precipitation and Hot Deformation Behavior of Austenitic Heat-Resistant Steels: A Review, *J. Mater. Sci. Technol.*, 2017, **33**, p 1448–1456
24. V.D. Vijayanand, K. Laha, P. Parameswaran, V. Ganesan, and M.D. Mathew, Microstructural Evolution During Creep of 316LN Stainless Steel Multi-pass Weld Joints, *Materials Science and Engineering: A*, 2014, **607**, p 138–144